Journal of Power Sources 225 (2013) 200–206

Contents lists available at SciVerse ScienceDirect

Journal of Power Sources

journal homepage: www.elsevier.com/locate/jpowsour

Electrochemical properties of Pt/graphene intercalated by carbon black and its application in polymer electrolyte membrane fuel cell

S.H. Cho, H.N. Yang, D.C. Lee, S.H. Park, W.J. Kim*

Department of Materials Chemistry and Engineering, Konkuk University, Neungdong-ro 126, Seoul 143-701, Republic of Korea

HIGHLIGHTS

- Carbon black (CB) was intercalated between graphene single nanosheets (GNSs).
- Pt/GNS shows the higher ECSA compared to Pt/CB and Pt/Vulcan XC-72 CB.
- Electrochemical active surface area depends on intercalating compound contents.
- Pt/GNS/CB with 30% of CB shows the highest ECSA of 38.8 $m^2\ g^{-1}$ with 400 mA cm^{-2}.

ARTICLE INFO

Article history:
Received 14 August 2012
Received in revised form
12 September 2012
Accepted 12 October 2012
Available online 23 October 2012

Keywords:
Graphene single nanosheet
Intercalation
Thermal exfoliation
Polymer electrolyte membrane fuel cell
Cell performance
Methanol oxidation

ABSTRACT

Graphene single nanosheet (GNS) is synthesized from graphite by chemical oxidation and thermal exfoliation at 1000 °C and confirmed by X-ray diffraction analysis. Scanning electron and transmission electron microscope images clearly show the lateral expansion of graphite sheet and uniform dispersion of Pt nanoparticles on GNS. Fourier transform infrared and X-ray photoelectron spectroscopy analyses are conducted for surface properties of GNS such as oxygenated functional groups. Cyclic voltammetric analysis shows that electrochemical active surface areas (ECSAs) for Pt/GNS, commercial Pt/Vulcan XC-72 carbon black and Pt-incorporated onto commercial carbon black (Pt/CB) prepared in the laboratory are 33.1 $m^2\ g^{-1}$, 23.5 $m^2\ g^{-1}$ and 22.5 $m^2\ g^{-1}$, respectively. Because of significant restacking of Pt/GNS sheets, carbon black (CB) with different content is intercalated between Pt/GNS as a spacer. The ECSAs of Pt/GNS, Pt/GNS/CB20, Pt/GNS/CB30 and Pt/GNS/CB40 are evaluated to be 31.5 $m^2\ g^{-1}$, 28.6 $m^2\ g^{-1}$, 38.8 $m^2\ g^{-1}$ and 30.4 $m^2\ g^{-1}$, respectively. The cell performance highly depends on CB content and Pt/GNS/CB with 30 wt.% of CB content shows the best cell performance of 400 mA cm^{-2}.

1. Introduction

Future energy concerns demand a transition from fossil fuels to energy resources which is more environmental friendly and durable. As an alternative energy source, polymer electrolyte membrane fuel cells (PEMFCs) have attracted a great attention as environmental energy technology for transportation vehicles, small-scale portable electronic and stationary power supplies [1]. Despite considerable progress in PEMFC, catalytic stability and durability still need to be improved [2]. In particular, carbon-supported electrocatalysts are important factor to upgrade the performance of PEMFCs [3,4]. Currently, carbon black (CB) is most widely used for support material, although it shows serious intrinsic corrosion under abnormal operating conditions. As one of alternative carbon supports, carbon nanotubes (CNTs) have received a huge amount of attention as an alternative carbon support material due to unique structural and electrical properties [5,6]. Another interesting alternative, carbon molecular sieve (CMS), has received attention due to prominent characteristics, such as high surface area, relatively uniform pore size and ordered pore structure [7]. Many researchers, however, have started to shift their research target toward graphene in the last few years after the existence of 2-dimensional graphene was reported [8–10]. Chen et al. [11] reported a great electrochemical performance of graphene single nanosheet (GNS) compared with graphene oxide (GO). Li et al. [12] reported that the performance of Pt/GNS for methanol oxidation has been proven to be superior to that of Pt supported on Vulcan XC-72 carbon black. The investigation of Pt/GNS about cell performance has been, however, limited up to now. In spite of excellent electrical conductivity of graphene, restacking of individual GNS has been a barrier as an effective carbon support because restacking would decrease the utilization

* Corresponding author. Tel.: +82 2 450 3502; fax: +82 2 444 8743.
E-mail address: whajungk@konkuk.ac.kr (W.J. Kim).

0378-7753/$ – see front matter © 2012 Elsevier B.V. All rights reserved.
http://dx.doi.org/10.1016/j.jpowsour.2012.10.040

of Pt active sites, making one side of Pt/GNS unavailable. In order to overcome this problem, Nafion ionomer can be added more but too much addition of it would make the electrode thickness, leading to the increase in mass transfer resistance and the decrease in electrical conductivity. Another way to overcome this problem is to intercalate CB between GNSs. The advantages of intercalation of CB are to prevent GNSs from restacking improving the accessibility of fuels to Pt active sites as well as mass transfer.

In this study, GNSs and Pt/GNS are synthesized through simple chemical oxidation of graphite followed by thermal exfoliation and the electrochemical and physical properties such as electrochemical active surface areas (ECSAs) and CO tolerance through methanol oxidation are also evaluated and compared with those of commercial Pt/Vulcan XC-72 CB and Pt/CB. Finally, the electrochemical properties of Pt/GNS/CB are evaluated and the cell performances of the membrane electrolyte assembly (MEA) fabricated with Pt/GNS and Pt/GNS/CB are also evaluated and discussed.

2. Experimental

2.1. Synthesis of GNSs

GNSs were synthesized by an easy method involving the steps of chemical oxidation of graphite and reduction by thermal exfoliation. GO, intermediate between graphite and GNSs was synthesized by modified Hummers method [13,14]. 2 g of graphite powder was added to a mixture of concentrated 50 ml of H_2SO_4, 2.5 g of $K_2S_2O_8$, 2.5 g of P_2O_5 (Aldrich). It was then stirred at 80 °C for 2 h. Subsequently, the mixture was cooled to room temperature for 6 h and diluted with distilled water (0.5 l) and dried overnight at room temperature. The pre-oxidized graphite was then re-oxidized. The pre-treated graphite powder was added to 35 ml of cold (0 °C) and concentrated H_2SO_4. Then, 6 g of $KMnO_4$ (Aldrich) was added slowly under stirring and the temperature of the mixture was kept below 20 °C in ice-bath. Successively, the mixture was stirred at 35 °C for 30 min, and then diluted with 100 ml of distilled water.

The mixture was then stirred at 95 °C for 30 min. The reaction was terminated by the addition of 150 ml of distilled water and 10 ml of 30 wt.% H_2O_2 solution in 15 min, after which the color of the mixture was changed to brilliant yellow along with bubbling. The mixture was filtered and washed with 100 ml of 10 wt.% HCl aqueous solution to remove metal ions followed by 500 ml of distilled water to remove the acid. The resulting GO powder was then obtained by high-speed centrifugation and drying in vacuum oven at 60 °C for 12 h. Reduction by thermal exfoliation of GO as prepared above was achieved by placing GO into tubular furnace at 1000 °C under Ar flow for 30 s [15,16]. After that, GNS was obtained and characterized.

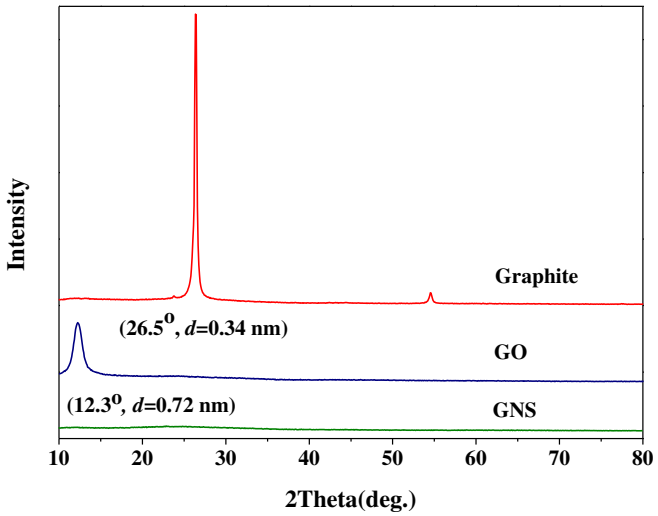

Fig. 1. XRD patterns of graphite, GO and GNS.

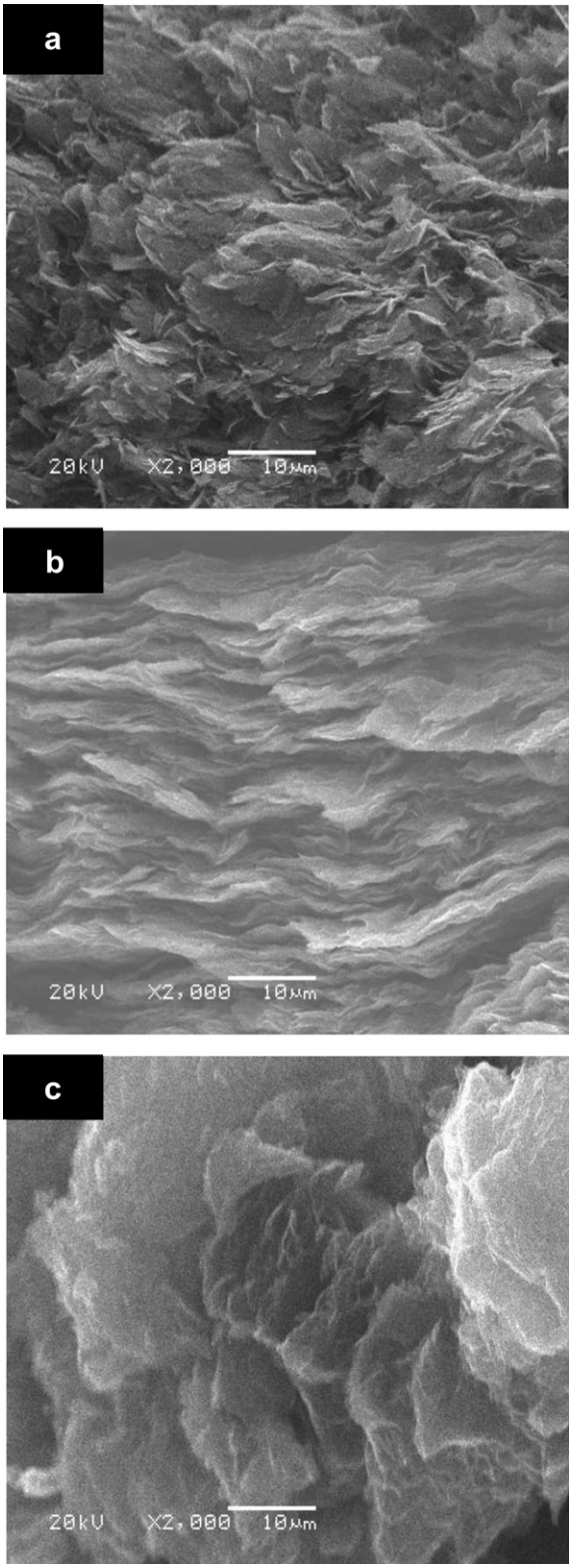

Fig. 2. SEM images of (a) graphite, (b) GO and (c) GNS.

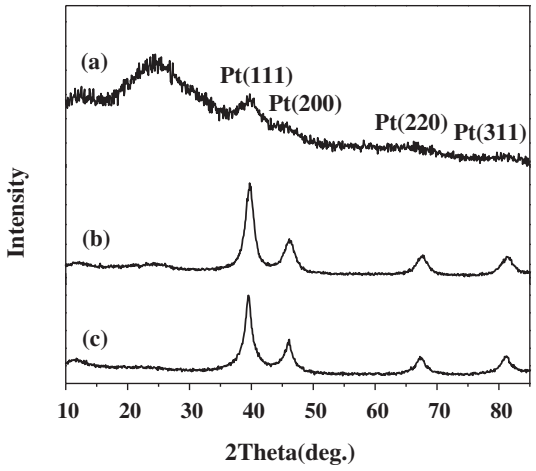

Fig. 3. XRD patterns of (a) Pt/GNS, (b) commercial Pt/Vulcan XC-72 CB and (c) Pt/CB.

2.2. Preparation of GNS-supported Pt nanoparticle catalyst

20 mg of GNS powder was dispersed in 20 ml of distilled water by sonication for 1 h, forming GNS suspension [17,18]. Then 40 ml of ethylene glycol and 1 ml of 0.02 M Pt precursor (water solutions of $H_2PtCl_6 \cdot 6H_2O$, Aldrich) were added to the solution under stirring for 1 h. Subsequently, the mixture was put in oil bath and heated at 100 °C for 24 h under stirring. The Pt/GNS was then separated from ethylene glycol solution in the centrifuge and washed with deionized water five times. The resulting products were dried in vacuum oven at 60 °C for 12 h.

2.3. Preparation of Pt/GNS intercalated by CB (Pt/GNS/CB)

In order to intercalate Pt/GNS by CB, the predetermined amounts of CB corresponding to 20 wt.%, 30 wt.% and 40 wt.% were added to 24 mg of Pt/GNS, followed by the addition of 85 mg of 5 wt.% Nafion™ dispersion (Dupont Chem. CO.). 1 ml IPA (99.5 wt.%, Samchun Chemicals) was then added and sonicated for 1 h at 50 °C.

2.4. Characterizations

2.4.1. Characterization of physical properties

Powder X-ray diffraction analyses (XRD, Rigaku Model D/Max 2200) were performed using Cu Kα radiation operating at 40 kV and 30 mA and scanning at a rate of 5° min^{-1} with an angular resolution of 0.04° of 2θ scan to get the XRD pattern. Scanning electron microscopy (SEM, JEOL JSM-6308) was conducted to investigate the morphology of graphite, GO and GNS. Transmission electron microscopy (TEM, 200 keV Carl Zeiss, EM 912 Omega) was conducted to identify dispersion and particle size. Thermal gravimetric analysis (TGA, Model TA2050 TA instruments) was conducted to confirm the Pt content in Pt/GNS. The Brunauer–Emmett–Teller (BET) surface area for as-made GNS was determined by nitrogen adsorption at 77 K from 0.01 to 0.05 in relative pressure (Micrometrics, Tristar™ II 3020). Atomic force microscope (AFM, Park systems XE-100) was also conducted to confirm the thickness of GNS obtained from thermal exfoliation. The pore diameter was determined by Barrett–Joyner–Halenda (BJH) desorption while the micropore volume was calculated from the Dubinin–Radushkevich equation. Fourier transform infrared spectroscopy (FT-IR) was used to confirm the presence of oxygenated groups. Finally, X-ray photoelectron spectroscopy (XPS, VG Multilab ESCA 2000) analysis was performed with Mg Kα radiation (1253.6 eV) to confirm the oxidation state of Pt nanoparticles and to characterize the formation of surface oxygenated groups on the obtained materials.

2.4.2. Electrochemical measurements

The ink slurry was prepared by sonicating cathode ink slurry. The same amount of ink slurry was dropped by micropipette onto glassy carbon electrode (GCE) with 3 mm in diameter and 0.0706 cm^2 in electrode area which was polished with 1 μm Al_2O_3 slurry to a mirror finish before being used as the substrate for carbon-supported catalyst. Cyclic voltammetric (CV) analysis was conducted in a conventional three electrode electrochemical cell using a GCE with 3 mm in diameter as a working electrode, Pt wire as a counter electrode and a saturated calomel electrode (SCE) as a reference electrode. Electrochemical measurements were recorded and reported vs. normal hydrogen electrode (NHE). The CVs were measured in N_2-purged 0.5 M H_2SO_4 electrolyte solution at 25 °C using a potentiostat and galvanostat (IM6, Zahner). The voltage was changed by a triangular wave between 0.05 V and 1.20 V at a scan rate of 50 mV s^{-1}, and the CV was then obtained. In order to characterize the electrochemical properties of fuel cell electrodes, fuel cell performance tests were performed.

For the cell performance test, anode and cathode were fabricated as follows. The catalyst ink was prepared to fabricate several electrodes using Pt/GNS and Pt/GNS/CBs with different contents of CB as follows. Pt/GNS synthesized by polyol method was first added to Nafion dispersion (5 wt.%, Dupont Chem. Co.) to which isopropyl

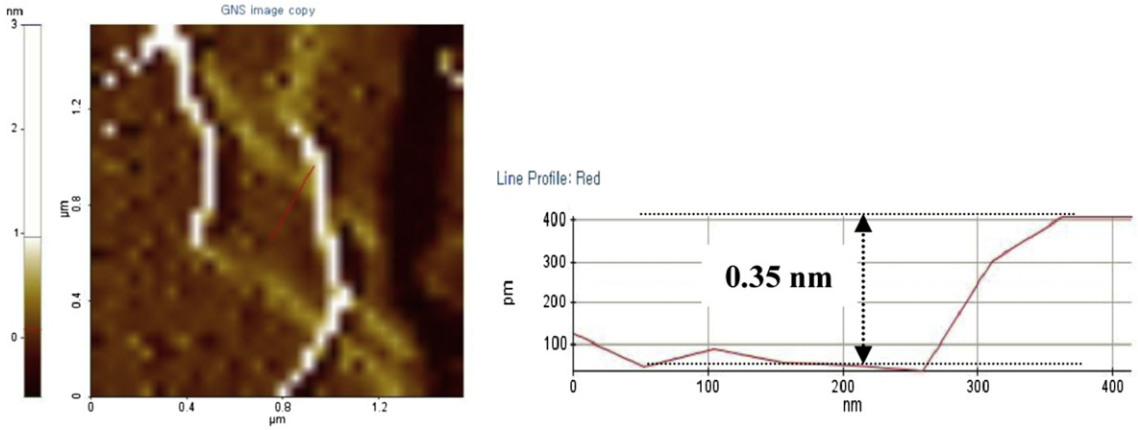

Fig. 4. AFM image of GNS for thickness measurement.

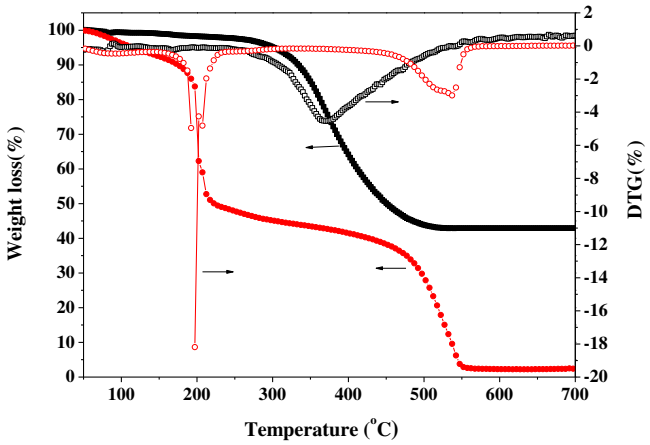

Fig. 5. TG/DTA curves of (■, □) Pt/GNS, and (●, ○) GO.

alcohol (IPA, 99.5 wt.%, Samchun Chemicals) as a solvent was sequentially added. To ensure the sufficient mixing, the catalyst ink was subject to 1 h of sonication. After preparing catalyst ink, it was brushed on a polymer electrolyte membrane (Nafion NRE-212, DuPont) of 3 × 3 cm^2 to gain Pt loadings of 0.2 mg cm^{-2} and 0.3 mg cm^{-2} at anode and cathode, respectively. During the measurements, the temperature of the single cell was maintained at 80 °C, and fully humidified hydrogen/oxygen gases were fed into the anode/cathode at 80 °C.

As a second set of experiment, another type of catalyst ink was prepared using Pt/GNS/CBx with different CB contents from 20 wt.% to 30 wt.% to 40 wt.%, following the same procedures as described above: that is, hereinafter denoted as Pt/GNS/CB20, Pt/GNS/CB30 and Pt/GNS/CB40, respectively. In all the cases, Nafion loadings were maintained at 0.25 mg cm^{-2} and 0.3 mg cm^{-2} for anode and cathode, respectively.

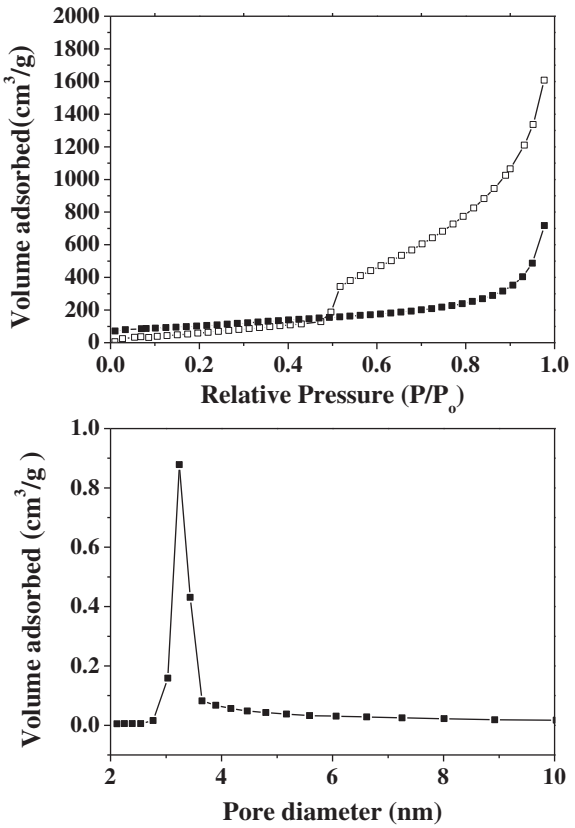

Fig. 6. N_2 adsorption isotherm and pore size distribution of as-made GNS.

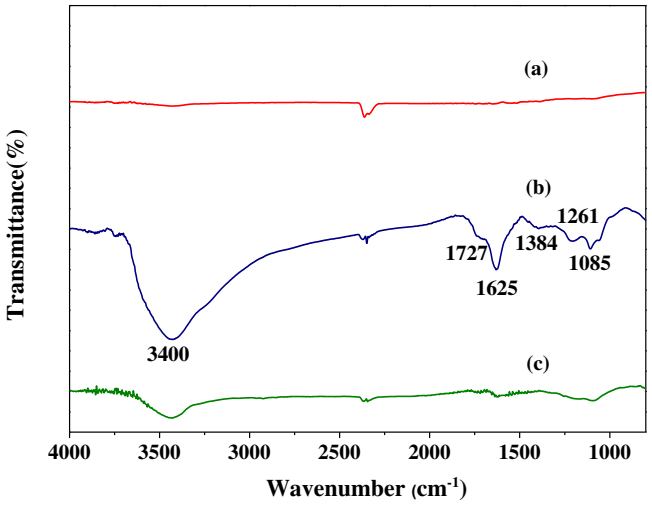

Fig. 7. FT-IR spectra of (a) graphite, (b) GO and (c) GNS.

3. Results and discussion

The XRD patterns of GNS obtained from modified Hummers method as described in experimental section are shown in Fig. 1. It shows the progressive phase change from graphite to GNS. Through chemical oxidation, a shift of C (002) peak at 26.5° in 2θ,

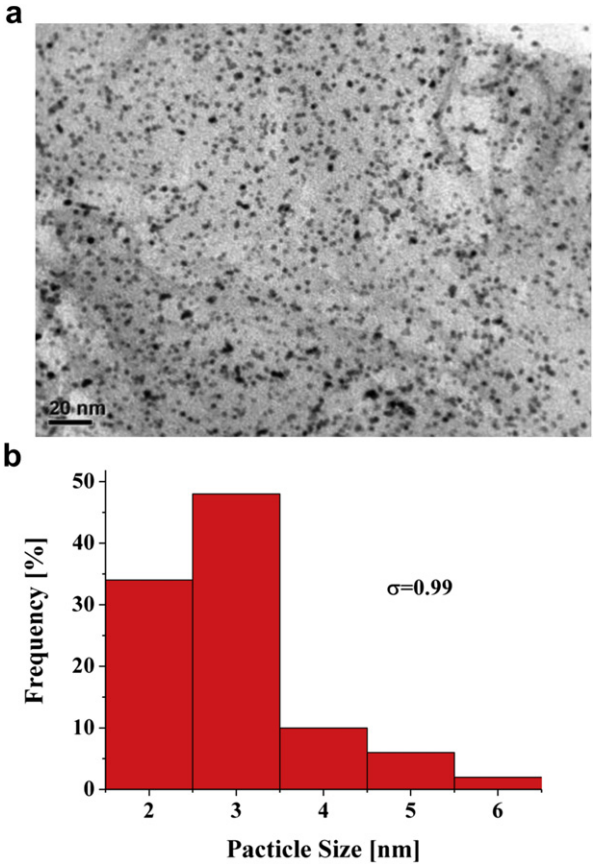

Fig. 8. TEM images of (a) Pt/GNS and (b) its particle size distribution.

characteristic of graphite to 12.3° in 2θ indicates that the stacked layers of graphite have been laterally expanded by the incorporation of oxygenated functional groups such as epoxy, carboxyl and hydroxyl groups, resulting in GO [15]. Then, the thermal reduction of GO led to GNS through the exfoliation of laterally expanded GO layers and the XRD pattern clearly indicates the formation of GNS by the disappearance of the peak around 12.3°, meaning the each layer of GO along c-axis was separated and carbon sp^2 structures were restored [16]. The disappearance of this peak is due to the lack of ordered stacked layers. In order to manifest the phase change, the SEM analysis was conducted and shown in Fig. 2. As can be seen in this figure, it is seen that bulky graphite materials have been expanded with apparent layer structure upon chemical oxidation.

As described in experimental section, Pt was incorporated onto GNS and identified by XRD if Pt was successfully incorporated. As shown in Fig. 3, apart from the peak at 24.5° assigned to GNS [19], the crystal structure of Pt is face-centered cubic (fcc), which is confirmed by the presence of diffraction peaks at 40°, 46°, 67.5° and 81.4° in 2θ assigned to Pt (111), Pt (200), Pt (220) and Pt (311), respectively. The average size of Pt particles was calculated from the (220) peak according to Scherrer equation as follows:

$$L = \frac{0.94}{B_{2\theta}} \frac{\lambda_{k\alpha 1}}{\cos\theta_B} \quad (1)$$

where L is the average particle size, the value 0.94 comes from spherical crystallite (cubo-octahedral shape). $\lambda_{k\alpha}$ is the X-ray wavelength radiation (1.54056 nm), $B_{2\theta}$ is the full width at half maximum (FWHM) in radians and θ_B is the angular position at the Pt (220) peak [20]. Based on the Scherrer equation with the FWHM for Pt (220), the average Pt particle size attached to GNS was estimated to be 2.5 nm, 3.47 nm and 3.50 nm, respectively.

To investigate if GNS was produced, AFM analysis was performed to measure the thickness of GNS and shown in Fig. 4. It is seen that the thickness of GNS is about 0.35 nm, consistent with that reported by Paredes et al. [21].

In addition, TGA was conducted to identify the Pt content in Pt/GNS. It was observed that Pt content on GNS was to be 42.9 wt.%. As shown in Fig. 5 for GO, the adsorbed water molecule was removed by 5% of weight loss up to 100 °C, followed by about 38% of weight loss at 200 °C due to the decomposition of labile oxygenated functional groups [22]. A weight loss around at 530 °C took place due to almost complete reduction of GO. Unlike GO, in case of GNS, no weight loss was observed around at 200 °C because most of oxygenated functional groups were already removed during reduction.

N_2 adsorption isotherm was measured to evaluate the surface area of GNS and shown in Fig. 6. A significant hysteresis observed is ascribed to irregular wrinkled structure of GNS, and the BET surface area was estimated to be 388 $m^2\ g^{-1}$ which is fairly enough for dispersion of Pt nanoparticles onto GNS. It should be noted, however, that the measured surface area is much smaller than the

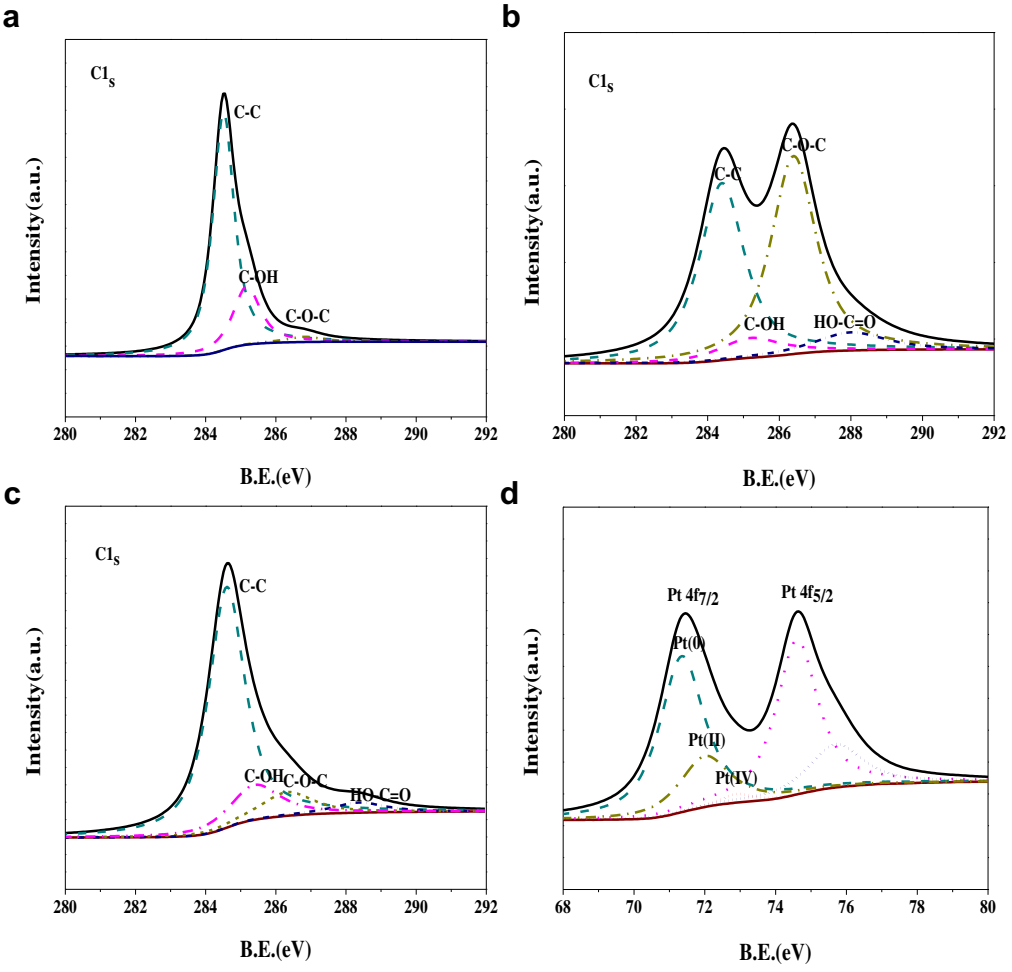

Fig. 9. XPS spectra of (a) graphite, (b) GO, (c) GNS and (d) Pt/GNS.

Table 1
Summary of sp^2-hybridized C–C and oxygenated functional groups for graphite, GO and GNS obtained from XPS analysis.

	C–C		C–OH		C–O–C		HO–C=O	
	B.E[a] (eV)	relative %	B.E (eV)	relative %	B.E (eV)	relative %	B.E (eV)	relative %
Graphite	284.5	72.5	285.2	22.7	286.8	2.8	288.0	2.0
GO	284.5	41.1	285.2	6.5	286.4	46.0	288.1	6.4
GNS	284.5	71.6	285.4	14.2	286.3	10.0	288.4	4.2

[a] B.E. represents binding energy (eV).

Table 2
Summary of oxidation states of Pt species for Pt/GNS obtained from XPS analysis.

Sample	Pt species on surface	Binding energy of Pt $4f_{7/2}$ (eV)	Relative intensity (%)
Pt/GNS	Pt(0)	71.4	54.8
	Pt(II)	72.4	29.8
	Pt(IV)	72.9	15.3

theoretical value because of restacking of GNS due to van der Waals forces [16].

In order to investigate the surface property change through the synthesis of GNS from graphite, FT-IR spectroscopy analysis was conducted and the results are shown in Fig. 7. Upon oxidation of graphite, GO was functionalized by the bending vibration of water molecules and OH stretching mode of the sorbed water molecules at 3400 cm^{-1}, carbonyl/carboxyl at 1727 cm^{-1}, aromatics at 1625 cm^{-1}, carboxyl at 1384 cm^{-1}, epoxy at 1261 cm^{-1} and alkoxy at 1085 cm^{-1}, respectively. It is clearly seen, however, that upon reduction by thermal exfoliation, most of these functional groups have been disappeared.

The TEM images of the dispersion of Pt/GNS with particle size distribution are shown in Fig. 8. It was observed that Pt nanoparticles on GNS were highly and uniformly dispersed and average Pt nanoparticle size was 2.9 nm.

In order to investigate the physical states of graphitic materials and the oxidation state of Pt for Pt/GNS, XPS analysis was conducted and the results are shown in Fig. 9 and summarized in Table 1. As seen in Fig. 9 (a), (b) and (c), four different types of carbon were resolved: those are, sp^2 hybridized C–C at 284.4 eV, C–OH at 285.3 eV, C–O–C at 286.4 eV and HO–C=O at 288.0 eV [16,23]. C–C peak in graphite was drastically decreased upon the oxidation shown in Fig. 9 (a) while oxygenated C–O–C was significantly increased shown in Fig. 9 (b).

Upon reduction through thermal exfoliation, the oxygenated functional groups were significantly decreased as shown in Fig. 9 (c). Therefore, it is said along with the XRD data that GNS has been successfully formed. Fig. 9 (d) represents the XPS spectra of Pt 4f doublet ($4f_{7/2}$ and $4f_{5/2}$) for the Pt nanoparticles supported on GNS. As can be seen in this figure, it shows the distribution of Pt(0), Pt(II), Pt(IV). The $4f_{7/2}$ and $4f_{5/2}$ peaks exhibited at 71.1 eV and 74.3 eV, respectively, which were slightly shifted to lower binding energy compared with standard binding energy of Pt $4f_{7/2}$ and $4f_{5/2}$ for Pt(0) state (71.4 eV and 74.5 eV) [24] due to the electron transfer from GNS to Pt nanoparticles [25]. Because the work function of GNS (4.48 eV) is smaller than that of Pt (5.65 eV) [26], electron transfer from GNS to Pt nanoparticles should have occurred during the formation of Pt/GNS hybrid structure. The oxidation states of various forms of Pt species for Pt/GNS are summarized in Table 2.

CVs of Pt/GNS were conducted to identify electrochemical active surface areas (ECSAs) of Pt on GNS. For comparison, commercial Pt/Vulcan XC-72 CB, and Pt/CB of which Pt was incorporated onto commercial CB in our lab were tested for ECSAs. The resulting CV curves are shown in Fig. 10. As seen in this figure, the peaks between 0.0 V and 0.3 V correspond to hydrogen adsorption/desorption and the double layer region between 0.3 V and 0.8 V corresponding to the region free of adsorbed hydrogen represents the characteristic of carbon material [27]. ECSAs for Pt nanoparticles deposited on GNS along with commercial Pt/Vulcan XC-72 CB and Pt/CB for comparison were calculated from hydrogen adsorption/desorption charge after correction for the double-layer charging current from the CV curves [28] according to the following equation.

$$\mathrm{ECSA}\left(m_{\mathrm{Pt}}^2/Q_{\mathrm{Pt}}\right) = \frac{\mathrm{Charge}\left(Q_{\mathrm{H}}C/m^2\right)}{210\left(\mu C/m_{\mathrm{Pt}}^2\right) \times \mathrm{Pt\ Wt.}\left(g_{\mathrm{Pt}}/m^2\right)} \quad (2)$$

ECSAs for Pt/GNS, commercial Pt/Vulcan XC-72 CB, Pt/CB were estimated to be 31.5 $m^2\ g^{-1}$, 23.1 $m^2\ g^{-1}$ and 22.5 $m^2\ g^{-1}$, respectively.

Finally, the cell performances of various MEAs assembled with various catalysts such as Pt/GNS and various Pt/GNS/CBs with different CB contents were evaluated and the results are shown in Fig. 11. It shows that the cell performance was significantly enhanced with the increase in CB content in catalyst from 20 wt.% to 30 wt.%. It is believed that the CB intercalated between GNSs should have enhanced the utilization of Pt active sites. It is

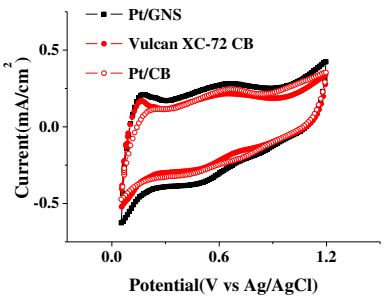

Fig. 10. CVs of Pt/GNS, commercial Pt/Vulcan XC-72 CB, and Pt/CB for ECSAs.

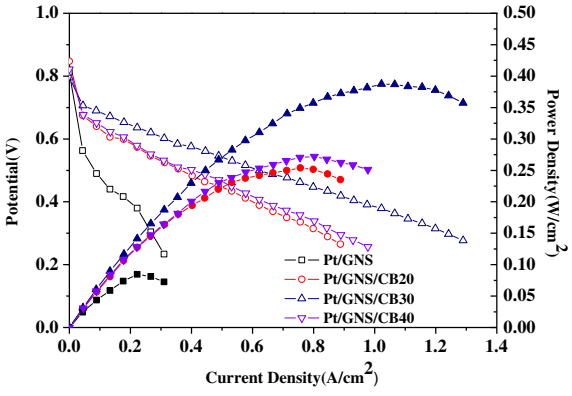

Fig. 11. Cell polarization curves of Pt/GNS, Pt/GNS/CB20, Pt/GNS/CB30 and Pt/GNS/CB40.

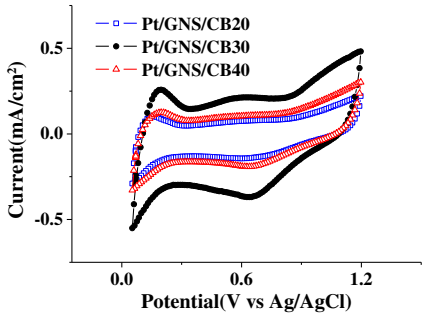

Fig. 12. CVs of Pt/GNS/CB20, Pt/GNS/CB30 and Pt/GNS/CB40 for ECSAs.

confirmed by the enhancement in power generation over entire current density: that is, enhanced activation at low current density and better mass transfer at high current density. Beyond 30 wt.% of CB content, however, the cell performance was rather decreased. It is ascribed to the fact that the excess of CB should have blocked Pt active sites, increasing mass transfer resistance.

In order to investigate the ECSAs of various Pt/GNS/CBx, CV curves were measured and shown in Fig. 12, respectively. Based on H_2 desorption peak, the ECSAs of Pt/GNS, Pt/GNS/CB20, Pt/GNS/CB30 and Pt/GNS/CB40 were evaluated to be 31.5 $m^2\ g^{-1}$, 28.6 $m^2\ g^{-1}$, 38.8 $m^2\ g^{-1}$ and 30.4 $m^2\ g^{-1}$, respectively. It is believed that there should be optimal CB content: that is, low CB content intercalated between GNSs is not enough to act as good spacer while too high CB content would block Pt active sites, decreasing the Pt utilization.

4. Conclusions

Through this study, GNS is successfully synthesized through chemical oxidation followed by thermal exfoliation at 1000 °C from graphite. The XRD pattern clearly shows the complete disappearance of C (200), indicating the formation of GNS which is also confirmed by AFM image where the thickness of GNS prepared in this study is 0.35 nm. It is also confirmed by FT-IR where a significant amount of oxygenated functional groups has been eliminated from GNS. Pt particle size attached to GNS is estimated to be 2.5 nm which is fairly consistent with that estimated from TEM. TEM image also clearly shows excellent dispersion of Pt nanoparticle onto GNS. XPS analysis also shows that upon thermal exfoliation, the amount of oxygenated functional groups has been drastically decreased. In addition, the ECSAs measured by the CV are in the order of Pt/GNS > commercial Pt/Vulcan XC-72 CB > Pt/CB.

The cell test using Pt/GNS and various Pt/GNS/CBx suggests that restacking problem is very critical as Pt/GNS is adopted in PEMFC. The cell test clearly indicates that the incorporation of CB into Pt/GNS would drastically enhance the cell performance in PEMFC due to the enhancement in mass transfer of fuel to Pt active sites, increasing the Pt utilization. It also suggests that the CB content is critical regarding the utilization of Pt active sites because too much intercalation of CB between GNSs would rather block the Pt active sites where ECSA of Pt/GNS/CB30 shows the maximum. In case of the MEA assembled with Pt/GNS catalyst which shows the highest ECSAs, the cell performance is highly poor compared to other MEAs with Pt/GNS/CBx because the restacking becomes severe during hot pressing for assembling of MEA, leading to significant mass transfer resistance and thus reducing Pt utilization.

Acknowledgment

This work was supported by the National Research Foundation of Korea (NRF) grant funded by the Korea government (MEST) (No. 2012R1A2A2A01013904).

References

[1] B.C.H. Steele, A. Heinzel, Nature 414 (2001) 345–352.
[2] J. Zhang, K. Sasaki, E. Shutter, R.R. Adzic, Science 315 (2007) 220–222.
[3] B. Seger, P.V. Kamat, J. Phys. Chem. C 113 (2009) 7990–7995.
[4] C.T. Hsieh, J.Y. Lin, J. Power Sources 188 (2009) 347–352.
[5] W.Z. Li, C.H. Liang, J.S. Qiu, W.J. Zhou, H.M. Han, Z.B. Wei, G.Q. Sun, Q. Xin, Electrochim. Acta 50 (2004) 791–794.
[6] J.B. Xu, K.F. Hua, G.Z. Sun, C. Wang, X.Y. Lv, Y.J. Wang, Electrochem. Commun. 8 (2006) 982–986.
[7] H. Nishihara, Q.H. Yang, P.X. Hou, M. Unno, S. Yamauchi, R. Saito, J.I. paredes, A. Martinez Alonso, J.M.D. Tascon, Y. Sato, M. Terauchi, T. Kyotani, Carbon 47 (2009) 1220–1230.
[8] K.S. Novoselov, A.K. Geim, S.V. Morozov, D. Jiang, Y. Zhang, S.V. Dubonos, I.V. Grigorieva, A.A. Firsov, Science 306 (2004) 666–669.
[9] K.S. Kim, Y. Zhao, H. Jang, S.Y. Lee, J.M. Kim, J.H. Ahn, P. Kim, J.Y. Choi, B.H. Hong, Nature 457 (2009) 706–710.
[10] D.A. Dikin, S. Stankovich, E.J. Zimney, R.D. Piner, G.H.B. Dommett, G. Evmenenko, S.T. Nguyen, R.S. Ruoff, Nature 448 (2007) 457–460.
[11] Y. Chen, X. Zhang, D. Zhang, P. Yu, Y. Ma, Carbon 49 (2011) 573–580.
[12] Y. Li, L. Tang, J. Li, Electrochem. Commun. 11 (2009) 846–849.
[13] W.S. Hummers, R.E. Offeman, J. Am. Chem. Soc. 80 (1958) 1339.
[14] X. Zhou, X. Huang, X. Qi, S. Wu, C. Xue, F.Y.C. Boey, Q. Yan, P. Chen, H. Zhang, J. Phys. Chem. C 113 (2009) 10842–10846.
[15] H.C. Schniepp, J.L. Li, M.J. McAllister, H. Sai, M. Herrera-Alonso, D.H. Adamson, R.K. Prud'homme, R. CarO, D.A. Savile, I.A. Aksay, J. Phys. Chem. B 110 (2006) 8535–8539.
[16] M.J. McAllister, J.L. LiO, D.H. Adamson, H.C. Schiepp, A.A. Abdala, J. Liu, M. Herrera-Alonso, D.L. Milius, R. CarO, R.K. Prud'homme, I.A. Aksay, Chem. Mater. 19 (2007) 4396–4404.
[17] S. Stankovich, D.A. Dikin, G.H.B. Dommett, K.M. Kohlhass, E.J. Zimney, E.A. Stach, R.D. Piner, S.T. Nguyen, R.S. Ruoff, Nature 442 (2006) 282–286.
[18] D. Li, M.B. Muller, S. Gilje, R.B. Kaner, G.G. Wallace, Nat. Nanotechnol. 3 (2008) 101–105.
[19] L. Tang, Y. Wang, Y. Li, H. Feng, J. Lu, J. Li, Adv. Funct. Mater. 19 (2009) 2782–2789.
[20] C.D. Wagner, L.E. Davis, M.V. Zeller, J.A. Taylor, R.H. Raymond, L.H. Gale, Surf. Interface Anal. 3 (1981) 211–215.
[21] J.I. Paredes, S. Villar-Rodil, P. Solis-Fernandez, A. Martinez-Alonso, J.M.D. Tascon, Langmuir 25 (2009) 5957–5968.
[22] W.F. Chen, L.F. Yan, P.R. Bangal, Carbon 48 (2010) 1146–1152.
[23] A.M. Puziy, O.I. Poddubnaya, R.P. Socha, J. Gurgul, M. Wisniewski, Carbon 46 (2008) 2113–2123.
[24] J.F. Moudler, W.F. Stickle, P.E. Sobol, K.D. Bomben, Handbook of X-ray Photoelectron Spectroscopy, Perkin Elmer, Eden Prairie, MN, 1992, pp. 235–236.
[25] X. Wu, Y. Pei, X.C. Zeng, Nano. Lett. 9 (2009) 1577–1582.
[26] H.B. Michaelson, J. Appl. Phys. 48 (1977) 4729–4733.
[27] A. Pozio, M. de Francesco, A. Cemmi, F. Cardellini, L. Giorgi, J. Power Sources 105 (2002) 13–19.
[28] Z.Q. Tian, S.P. Jiang, Y.M. Liang, P.K. Shen, J. Phys. Chem. B 110 (2006) 5343–5350.